Electronic Supplementary Material (ESI) for Journal of Materials Chemistry A.

Supporting Information

Terminal Group Engineering for Small-Molecule Donor Boosts the Performance of Nonfullerene Organic Solar Cells

Tainan Duan,[†] Hua Tang,[†] Ru-Ze Liang,[*] Jie Lv, Zhipeng Kan,[*] Ranbir Singh, Manish Kumar, Zeyun Xiao, Shirong Lu[*] and Frédéric Laquai

Content:

1. General Experimental Details

All reactions were performed under nitrogen atmosphere and solvents were purified and dried from appropriate drying agents using standard techniques prior to use. Reagents available from commercial sources were used without further purification unless otherwise stated. Flash chromatography was performed by using Silicycle Silica Flash P60 (particle size 40-63 μm, 60 Å, 230-400 mesh) silica gel. Silica gel on TLC-PET foils from Fluka was used for TLC. The (4,8-bis(5-(2-ethylhexyl)thiophen-2-yl)benzo[1,2-b:4,5-b']dithiophene-2,6-diyl)bis(trimethylstannane) that used to synthesize the intermediate **3** was purchased from Derthon Optoelectronic Materials Science Technology Co., Ltd. All compounds were characterized by NMR spectroscopy on Bruker Avance III Ultrashield Plus instruments (600 MHz). The spectra were referenced on the internal standard TMS. High-resolution mass spectrometry (HRMS) data was recorded using a Thermo Scientific-LTQ Velos Orbitrap MS. Note: Spectroscopy-grade $CHCl_3$ was filtered through basic alumina prior to use in order to suppress solvent acidity and avoid undesired protonation reactions that may influence the spectral absorption of the molecular acceptors described in this study.

2. Synthetic Protocols and Characterizations

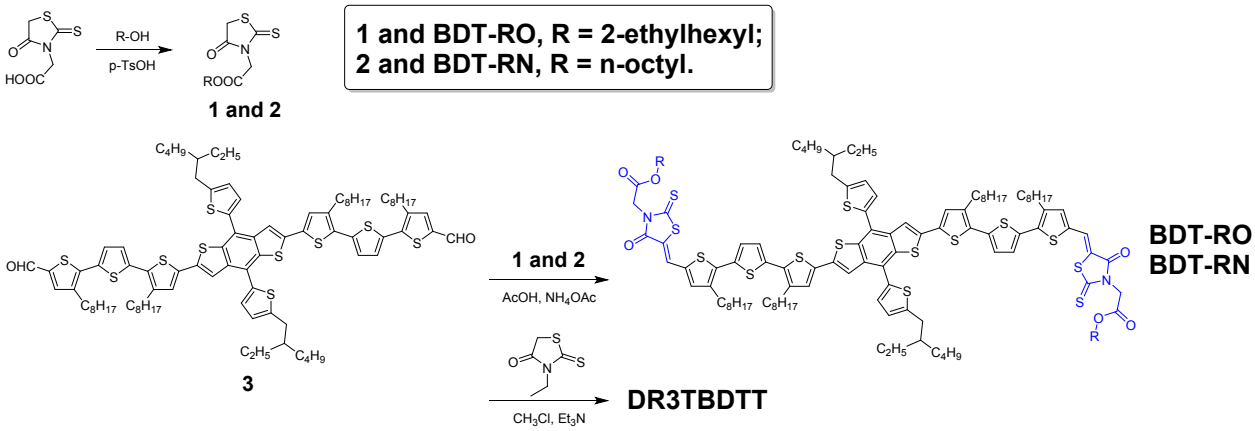

Scheme S1. Synthetic routes of the esterified rhodanine and SM donors.

Note: Compound **3**[1], **DR3TBDTT**[1] and SM acceptor **IDIC**[2] were prepared according to previously report procedures.

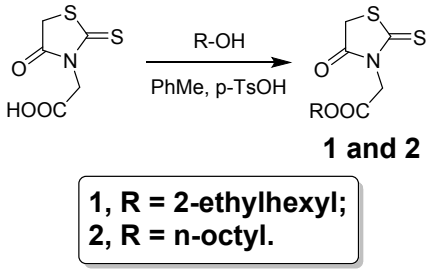

General procedure for the preparation of the terminal group 1 and 2: Rhodanine-3-acetic acid (1.0 equiv.), alcohol (2-ethylhexanol or 1-octanol, 1.0 equiv.) and p-Toluenesulfonic acid monohydrate (0.05 equiv.) were added into a solution of anhydrous toluene (≈ 50 mL), and the mixture was heated to refluxing and stirred for 12 h (a Dean-Stark apparatus was used to remove the water generated during the reaction). The reaction mixture was allowed to cool down to room temperature, filtered and was concentrated under reduced pressure. The crude product was purified by column chromatography over SiO_2 using DCM/hexanes (2:1) as the eluent. The solvent was removed by rotary evaporation, affording the desired terminal group (**1** or **2**) as a yellow oil.

1 (yield: 95%): ^{1}H NMR (600 MHz, $CDCl_3$, δ ppm): 4.74 (s, 2H), 4.11-4.09 (m, 4H), 1.60-1.59 (m, 1H), 1.36-1.29 (m, 8H), 0.93-0.89 (m, 6H). ^{13}C NMR (150 MHz, $CDCl_3$, δ ppm): 200.42,

173.01, 165.86, 68.26, 44.88, 38.74, 35.58, 30.34, 28.85, 23.76, 22.93, 13.98, 10.94. HRMS (+APCI, m/z): calcd. for $C_{13}H_{21}NO_3S_2$ $[M+H]^+$: 304.10356, found 304.10521.

2 (yield: 97%): ^{1}H NMR (600 MHz, $CDCl_3$, δ ppm): 4.73 (s, 2H), 4.17 (t, J = 6.6 Hz, 2H), 4.09 (s, 2H), 1.66-1.64 (m, 2H), 1.34-1.30 (m, 10H), 0.90 (t, J = 6.6 Hz, 3H). ^{13}C NMR (150 MHz, $CDCl_3$, δ ppm): 200.57, 173.06, 165.84, 66.11, 44.85, 35.64, 31.71, 29.10, 29.07, 28.45, 25.72, 22.59, 14.05. HRMS (+APCI, m/z): calcd. for $C_{13}H_{21}NO_3S_2$ $[M+H]^+$: 304.10356, found 304.10483.

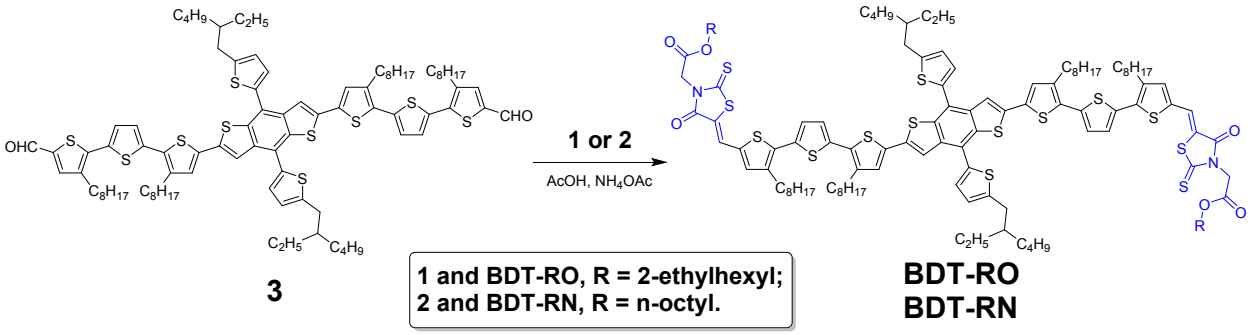

General procedure for the preparation of the terminal group 1 and 2: The aldehyde **3** (1.0 equiv.), esterified rhodanine (1 or 2, 6.0 equiv.) and NH_4OAc (0.1 equiv.) were added into a solution of acetic acid (≈ 30 mL), and the mixture was heated to 120 °C and stirred for 24 h. The reaction mixture was allowed to cool down to room temperature, was filtered and washed with ethyl acetate (2 × 20 mL), affording the desired products in high yield (> 90%) and high purity. Further purification can be performed via recrystallization in ethyl acetate.

BDT-RO: Purple-blue solid (yield, 90%). ^{1}H NMR (600 MHz, $CHCl_3$, δ ppm): 7.84 (s, 2H), 7.64 (s, 2H), 7.35 (d, J = 3.0 Hz, 2H), 7.26-7.24 (m, 4H), 7.14-7.13 (m, 4H), 6.98 (d, J = 3.0 Hz, 2H), 4.86 (s, 4H), 4.12 (d, J = 5.4 Hz, 4H), 2.95-2.93 (m, 4H), 2.84 (t, J = 7.2 Hz, 4H), 2.79 (t, J = 7.2 Hz, 4H), 1.77-1.70 (m, 12H), 1.53-1.29 (m, 72H), 1.04-0.97 (m, 12H), 0.91-0.89 (m, 24H). ^{13}C NMR(150 MHz, $CHCl_3$, δ ppm): 191.77, 166.64, 165.98, 145.93, 140.96, 140.84, 139.90, 138.61, 137.71, 137.55, 137.28, 136.87, 135.59, 134.84, 134.62, 130.46, 128.23, 127.90, 127.20, 126.00, 125.59, 125.47, 123.24, 119.75, 119.10, 68.20, 44.93, 41.56, 38.75, 34.44, 32.64, 31.93, 31.89, 30.41, 30.39, 30.17, 29.83, 29.75, 29.61, 29.57, 29.51, 29.47, 29.33, 29.29, 29.03, 28.87, 25.94, 23.79, 23.11, 22.96, 22.69, 22.67, 14.24, 14.10, 14.09, 14.00, 11.03, 10.97. HRMS (+APCI, m/z): calcd. for $C_{118}H_{156}N_2O_6S_{14}$ $[M+H]^+$: 2145.81261, found 2145.81496.

BDT-RN: Purple-blue solid (yield, 92%). ^{1}H NMR (600 MHz, $CHCl_3$, δ ppm): 7.83 (s, 2H), 7.62 (s, 2H), 7.35 (d, J = 3.0 Hz, 2H), 7.25-7.23 (m, 4H), 7.13-7.12 (m, 4H), 6.98 (d, J = 3.0 Hz, 2H), 4.85 (s, 4H), 4.19 (t, J = 6.6 Hz, 4H), 2.95-2.93 (m, 4H), 2.84 (t, J = 7.2 Hz, 4H), 2.79 (t, J = 7.2 Hz, 4H), 1.78-1.65 (m, 14H), 1.53-1.30 (m, 76H), 1.04 (t, J = 7.2 Hz, 6H), 0.98 (br, 6H), 0.91-0.89 (t, J = 7.2 Hz, 18H). ^{13}C NMR(150 MHz, $CHCl_3$, δ ppm): 191.74, 166.56, 165.95, 145.75, 140.72, 140.57, 140.00, 138.45, 137.71, 137.53, 137.16, 137.07, 136.96, 135.45, 134.64, 134.51, 130.47, 128.08, 127.92, 127.00, 125.72, 125.54, 125.43, 123.05, 119.57, 118.96, 66.03, 44.87, 41.56, 34.45, 32.67, 31.97, 31.93, 31.78, 30.37, 30.10, 29.95, 29.87, 29.70, 29.66, 29.57, 29.53, 29.40, 29.35, 29.18, 29.14, 29.05, 28.49, 25.95, 25.78, 23.15, 22.73, 22.71, 22.65, 14.29, 14.13, 14.12, 14.09, 11.07. HRMS (+APCI, m/z): calcd. for $C_{118}H_{156}N_2O_6S_{14}$ $[M+H]^+$: 2145.81261, found 2145.81530.

3. UV-Vis Absorption Spectra

UV-Vis absorption spectra of BDT-RO and BDT-RN were recorded on PerkinElmer LAMBDA 365 UV-Vis spectrophotometer.

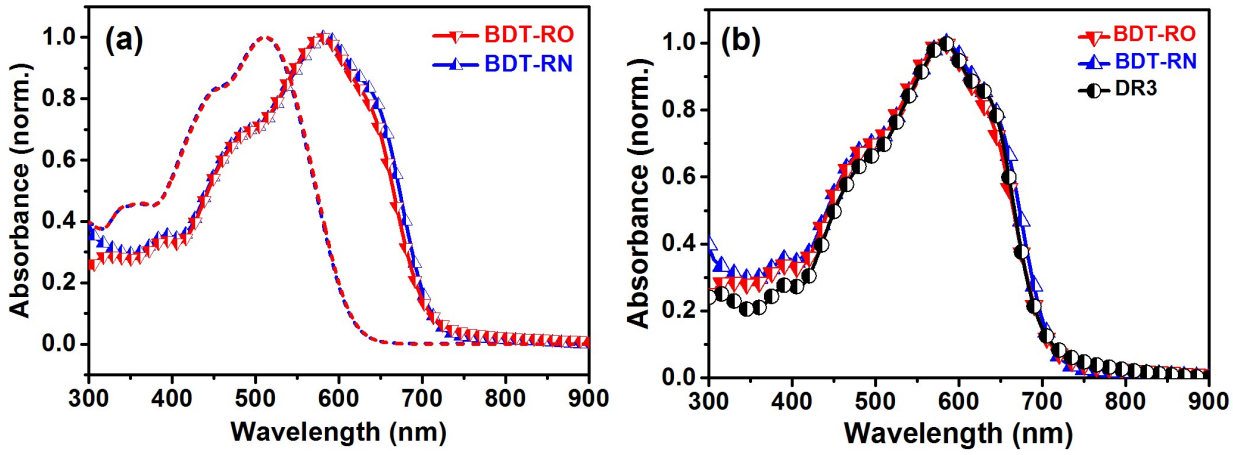

Figure S1. **(a)** Normalized solution (3.0×10^{-5} M in chloroform) (short dash) and thin-film (solid line with symbol) UV-vis absorption spectra of the two SM donors; (b) Normalized thin-film UV-vis absorption spectra of all three SM donors used in this work.

4. Energy Level Diagram

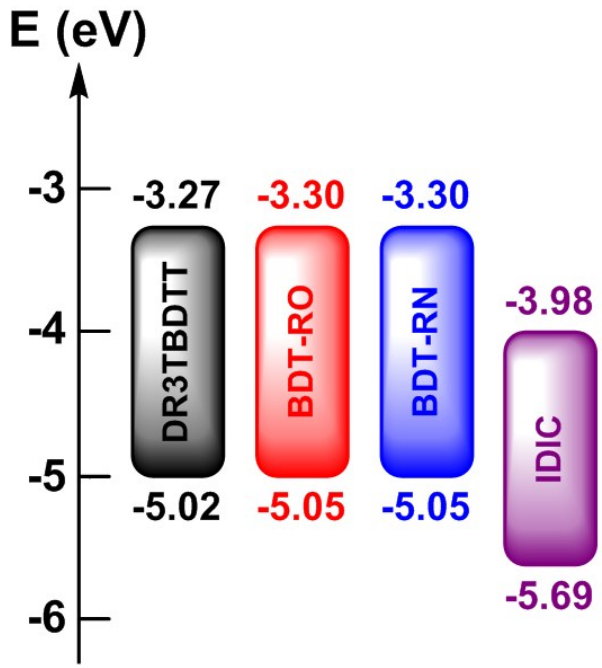

Figure S2. Energy level diagram of the SM donors and SM acceptor IDIC used in this work.

5. Differential Scanning Calorimetry (DSC) Measurements

Differential Scanning Calorimetry (DSC) measurements were performed on a Mettler-Toledo TGA/DSC 3+ analyzer under a nitrogen atmosphere, using aluminum crucibles.

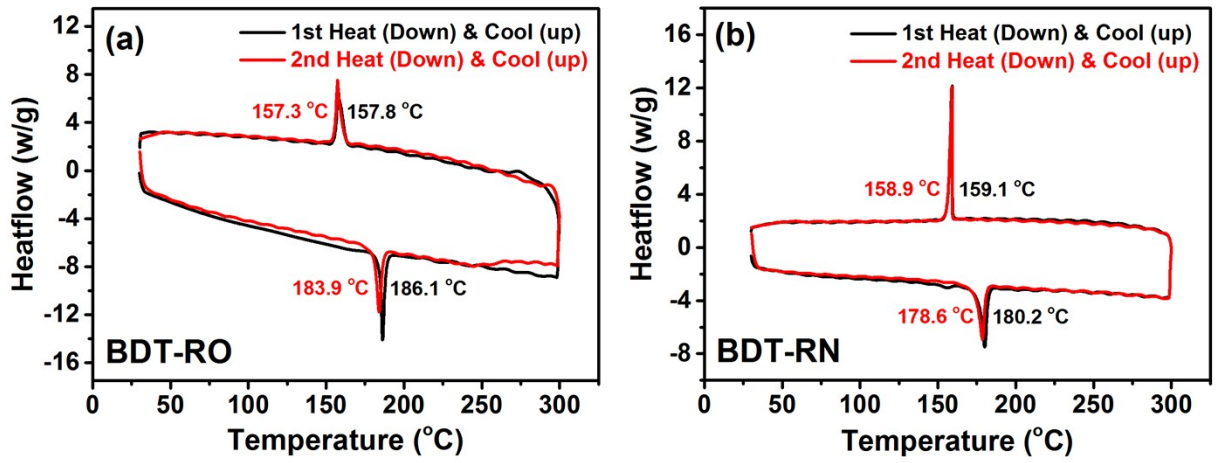

Figure S3. Differential Scanning Calorimetry (DSC) traces of **(a) BDT-RO** and **(b) BDT-RN**. Analyses carried out with a scan rate of 10 °C/min between 30 °C and 300 °C. Both molecular acceptors show an apparent phase transition around 180 °C, suggesting a melt transition in light of the presence of a first order solidification peak on the cooling scan.

6. Device Fabrication

The BHJ solar cells were prepared on glass substrates with tin-doped indium oxide (ITO, 15 Ω/sq) patterned on the surface (device area: 0.1 cm^2). Substrates were prewashed with isopropanol to remove organic residues before immersing in an ultrasonic bath of dilute Extran® 300 for 15 min. Samples were rinsed in flowing deionized water for 5 min before being sonicated (Branson 5510) for 15 min each in successive baths of deionized water, acetone and isopropanol. Next, the samples were dried with pressurized nitrogen before being exposed to a UV-ozone plasma for 20 min. A thin layer of PEDOT:PSS (~35nm) (Clevios AL4083) was spin-coated onto the UV-treated substrates, the PEDOT-coated substrates were subsequently annealed on a hot plate at 150 °C for 15 min, and the substrates were then transferred into the glovebox for active layer deposition.

All solutions were prepared in the glovebox using the SM donor (BDT-RO or BDT-RN) and the SM acceptor IDIC; the SM donors BDT-RO and BDT-RN were synthesized as mentioned above. The IDIC was purchased from Suna Tech Inc., Inc. Optimized devices were obtained by dissolving BDT based donor and IDIC in chloroform (CF) using a BDT based donor: IDIC ratio of 1:0.8 (wt/wt), total concentration of 18mg/ml. Note: The as-prepared solutions were stirred for 3 hours at 50 °C before being spin coat on the (room temperature) substrates. The active layers were spin-coated from the solutions at 50 °C at an optimized speed of 3000 rpm for time period of 45s, using a programmable spin-coater from Specialty Coating Systems (Model G3P-8), resulting in films of 130 to 140 nm in thickness. The active layers were then exposed to solvent vapor annealing (SVA) with carbon disulfide (CS_2) vapors for 20s. The effects of various solvents and duration on device performance were also examined.

Following SVA treatment, a ~10nm-thin layer of Phen-NaDPO was coated atop. The samples were then dried at room temperature for 1 hour. Next, the samples were placed in a thermal evaporator for evaporation of a 100 nm-thick layer of Silver (Ag) evaporated at 1 Å s^{-1}; pressure of less than $2x10^{-6}$ Torr. Following electrode deposition, samples underwent J−V testing.

J-V measurements of solar cells were performed in the glovebox with a Keithley 2400 source meter and an Oriel Sol3A Class AAA solar simulator calibrated to AM 1.5 G, with a KG-5 silicon reference cell certified by Newport. The external quantum efficiency (EQE) measurements were performed at zero bias by illuminating the device with monochromatic light

supplied from a Xenon arc lamp in combination with a dual-grating monochromator. The number of photons incident on the sample was calculated for each wavelength by using a silicon photodiode calibrated by NIST.

7. Additional PV Device Performance Data

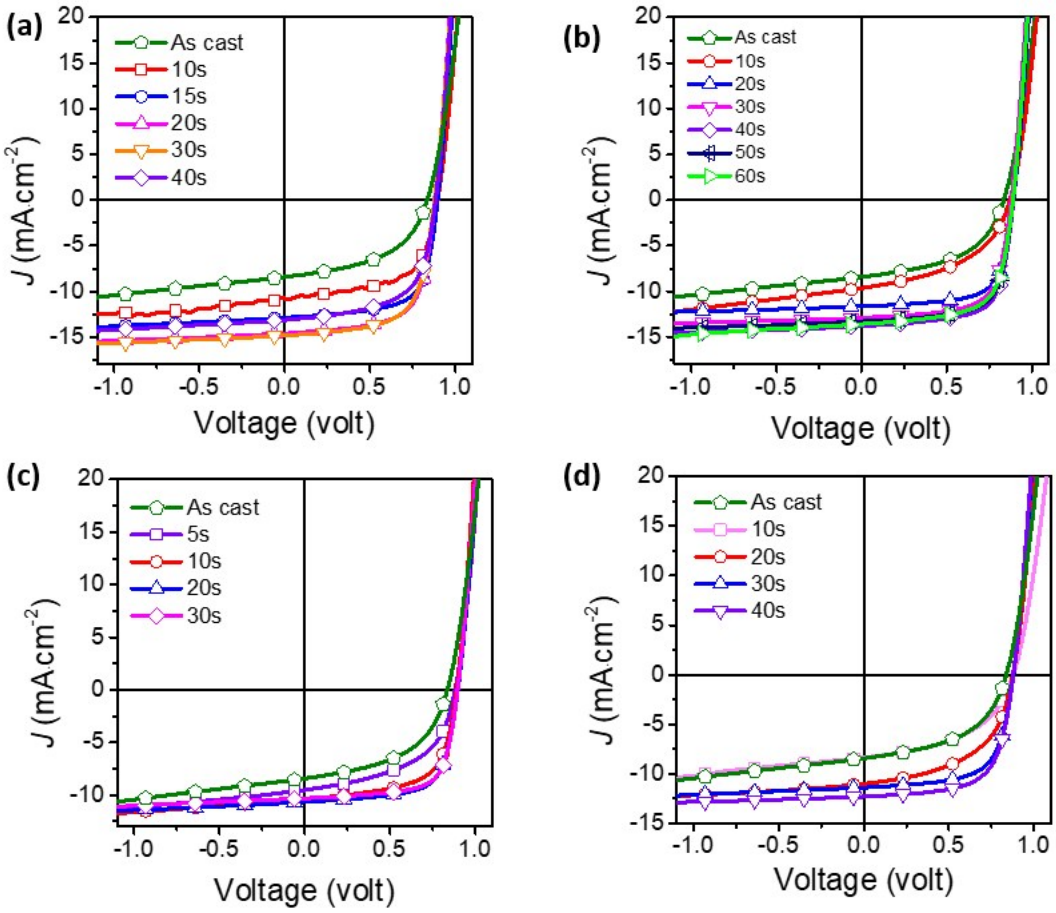

Figure S4. *J-V* curves of BHJ solar cells based on BDT-RO:IDIC active layers spin-coat from CF solution at the D/A ratio of 5:5, and subjected to various SVA treatments with varying solvents and exposure times. (a) SVA of BHJ solar cells with CS_2 and various exposure times. (b) SVA of BHJ solar cells with THF and various exposure times. (c) SVA of BHJ solar cells with CF and various exposure times. (b) SVA of BHJ solar cells with DMDS various exposure times.

Table S1. Summary of average PV performance for BDT-RO:IDIC active layers cast from CF solution at the optimized D/A ratio of 5:5, and subjected to various SVA treatments with varying solvents and exposure times. All current densities are in mA cm^{-2}

Solvent	SVA [s]	V_{OC} [V]	J_{SC} [mA cm^{-2}]	*FF* [%]	Avg. PCE [%]	Max. PCE [%]
CS_2	0	0.87	8.66	50.93	3.24	3.82
	10	0.90	10.76	60.59	5.65	5.85
	15	0.90	12.89	67.87	7.62	7.84
	20	0.88	14.62	67.02	8.55	8.64
	30	0.88	14.83	65.63	8.42	8.55
	40	0.89	13.14	61.44	7.02	7.15
THF	0	0.87	8.66	50.93	3.24	3.82
	10	0.87	9.65	47.12	3.62	3.97
	20	0.89	11.73	69.23	6.98	7.19
	30	0.88	12.90	68.01	7.56	7.72
	40	0.89	13.81	69.25	8.42	8.53
	50	0.89	13.29	69.18	8.01	8.19
	60	0.89	13.59	66.62	7.85	8.06
CF	0	0.87	8.66	50.93	3.24	3.82
	5	0.88	9.53	61.47	4.06	4.33
	10	0.89	10.39	62.90	5.66	5.82
	20	0.90	10.66	68.27	6.42	6.54
	30	0.90	10.32	69.97	6.05	6.47
DMDS	0	0.87	8.66	50.93	3.24	3.82
	10	0.88	8.35	48.62	3.20	3.56
	20	0.87	11.00	52.37	4.76	5.04
	30	0.88	11.38	65.72	6.35	6.57
	40	0.88	12.28	65.77	6.86	7.09

8. Light-Intensity Dependence Analyses

The light-intensity dependence measurements were performed with PAIOS instrumentation (Fluxim) (characterizations in steady-state and transient modes). A function generator controls the light source- a white LED with 200 mW cm-2 of maximum light intensity (rise/fall time 100 ns). A second function generator controls the applied voltage. The current and the voltage of the solar cell are measured with a digitizer. The current is measured via the voltage drop over a 20 Ω resistor or a transimpedance amplifier, depending on the current amplitude. In accounting for spectral mismatch, 100% of the maximum irradiance of the white-light LED was used to reproduce the JSC values normally achieved under standard AM1.5G solar illumination (100mW/cm2) and represent 1 sun equivalent.

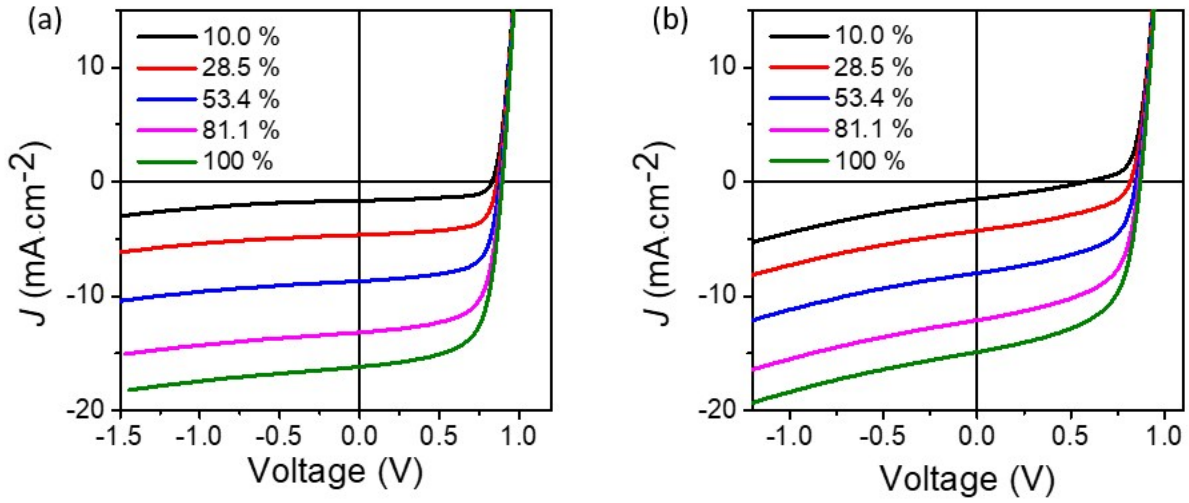

Figure S5. J-V curves of BHJ solar cells made with (a) BDT-RO:IDIC=1:0.8 and (b) BDT-RN:IDIC=1:0.8 under five different light intensities: 10%, 28.5%, 53.4%, 81.1% and 100% of one-sun equivalent.

9. Photoluminescence (PL) Quenching

Samples for PL spectroscopy were spin-coated onto glass substrates using the optimized conditions developed for the BHJ solar cells (BDT based donor:acceptor=1:0.8(wt/wt), total concentration of 18mg/ml, SVA of CS_2 for 20s.). Spectra were measured using a spectrofluorometer FluoroMax-4, HORIBA.

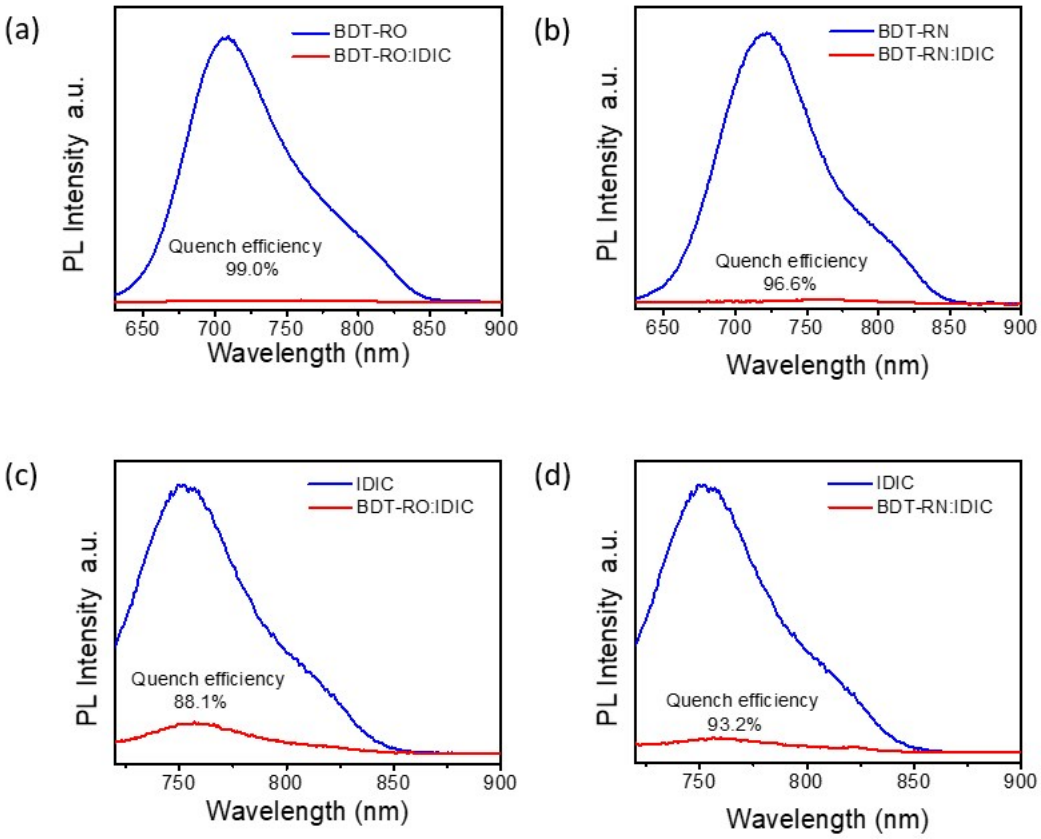

Figure S6. Photoluminescence (PL) quenching for neat films of **BDT-RO**, **BDT-RN** and **IDIC** and for optimized **BDT-RO:IDIC**, **BDT-RN:IDIC** BHJ thin films. (a) Excitation at the **BDT-RO**(580nm); (b) Excitation at the **BDT-RN**(580nm). PL quenching for neat films of **BDT-RO** and **BDT-RN**, and optimized **BDT-RO:IDIC**, **BDT-RN:IDIC** BHJ thin films. (c), (d) Excitation at **the IDIC**(710nm). PL quenching for neat films of **IDIC** and optimized **BDT-RO:IDIC**, **BDT-RN:IDIC** BHJ thin films.

10. Atomic Force Microscopy (AFM) Imaging

A Dimension Icon atomic force microscope (AFM) from Bruker was used to image the active layers in tapping mode (heights and phase images are represented below). A high aspect ratio antimony-doped Si cantilever with a spring constant of 1 - 5 (N m-1) (SCM-PIT, Veeco) was used for the analyses.

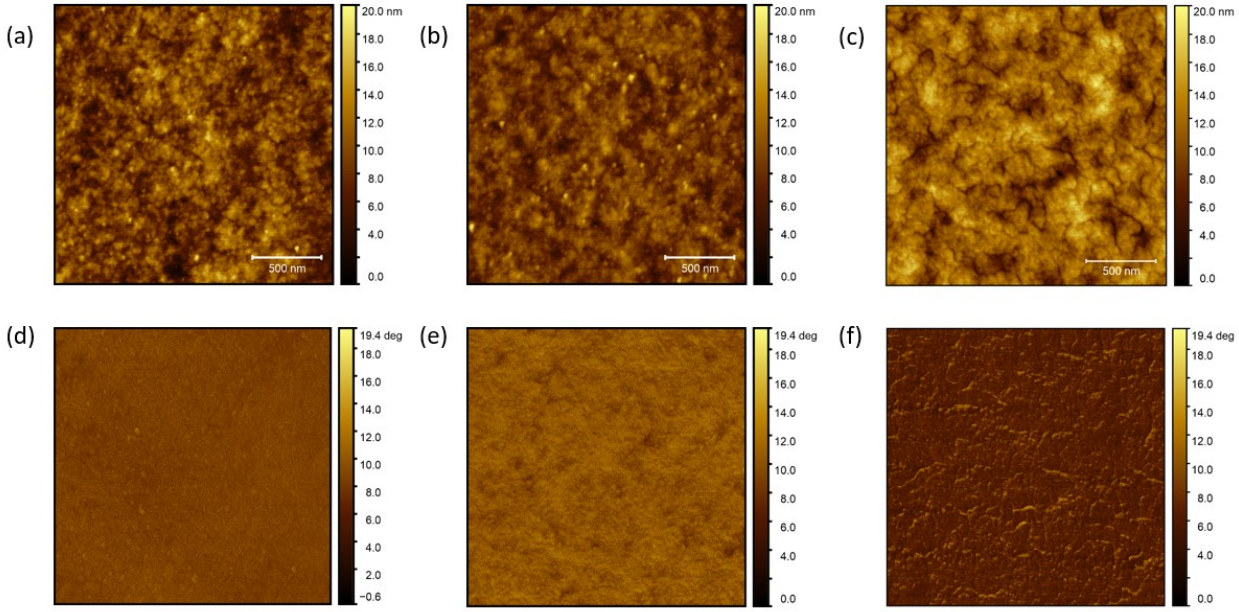

Figure S7. AFM images (2x2 μm^2) of (a, b, c) topography and (d, e, f) phase mode for **BDT-RO:IDIC, BDT-RN:IDIC** and **DR3TBTT:IDIC** BHJ films. (a, d) BHJ film of **BDT-RO:IDIC,** RMS roughness: 2.34nm; (b, e) BHJ film of **BDT-RN:IDIC**, RMS roughness: 1.87nm; (c, f) BHJ film of **DR3TBTT:IDIC**, RMS roughness: 2.28nm.

11. Electron Energy Loss (EELS) Characterization

Films were spun-cast on PEDOT:PSS-coated glass substrates. The BDT based donor:IDIC BHJ films were floated off the substrates in deionized water and collected on lacey carbon coated TEM grids (Electron Microscopy Sciences). TEM studies in a combination with EELS were performed a Thermo Fischer (former FEI) Titan Titan 80-300 TEM equipped with an electron monochromator and a Gatan Imaging Filter (GIF) Quantum 966. The microscope was operated at 80 kV to minimize electron beam induced damages of polymers and to increase EELS signal/noise ratio. The EELS maps were acquired in Scanning TEM (STEM) mode as so-called spectrum imaging (SI). To resolve spectral features clearly the monochromator was exploited to obtain energy resolution of 150meV.

Each material (component) used in this study in its neat form has a distinct signature or features of the EELS structure in the range from 1 to 8eV (see the comparison of these features in Fig.S8a). In the range from 1 to 5eV, these features result from so called inter-band transitions and have the same physical origin (related to the zone structure) as those in the UV-vis absorption spectra (Fig. 1a). Importantly, the low loss EELS structure of IDIC is significantly different compared to that of the donor BDT-RO and BDT-RN. Those key differences allow for a reliable fitting (as a linear combination) of the signatures from the individual components into the EELS obtained from the component mix. Essentially, the maps constructed this way – from the fitting coefficients –represent the distribution of the components over the blended specimen.

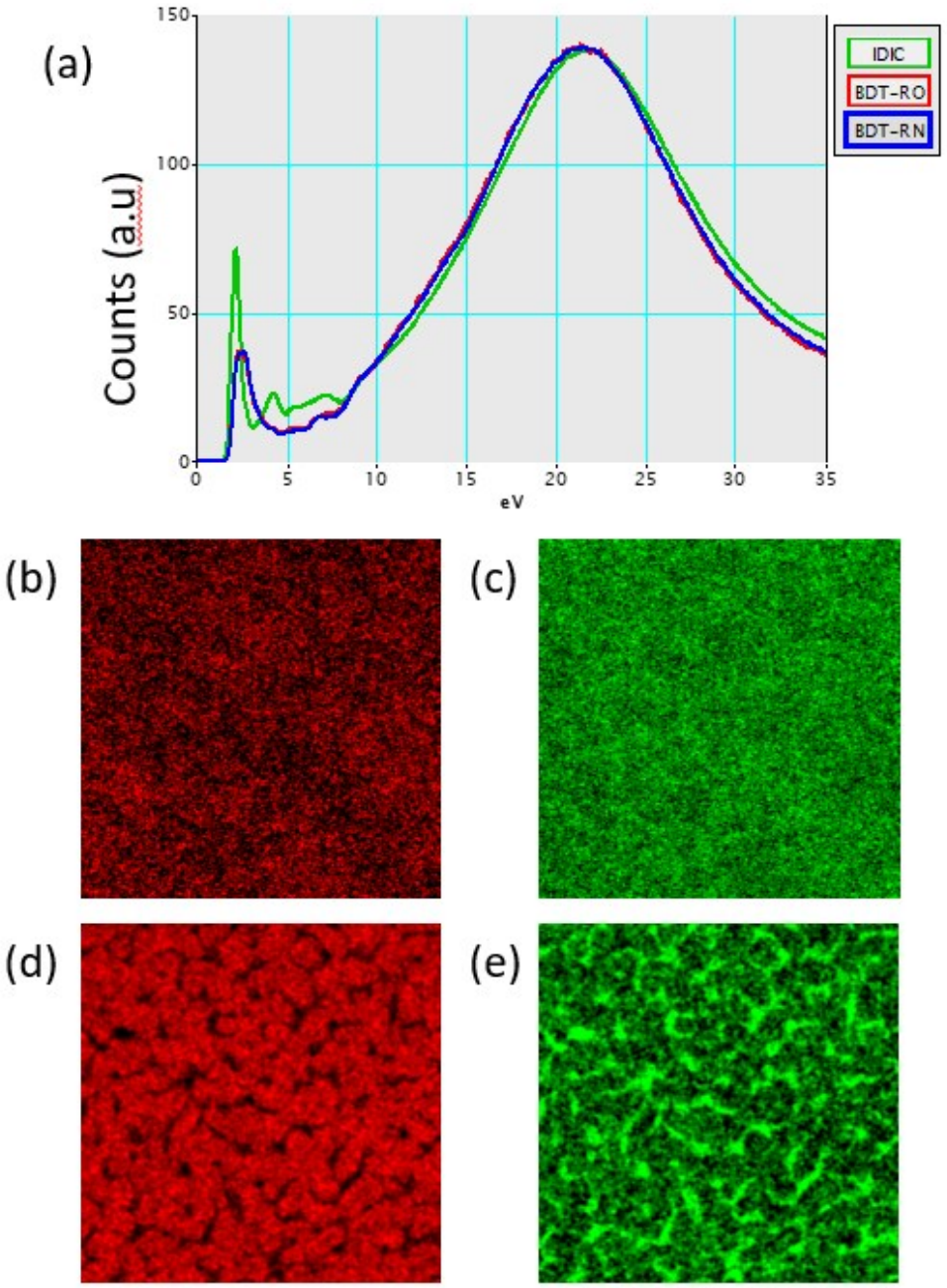

Figure S8. Characterization of BDT-RO:IDIC, BDT-RN:IDIC BHJ thin-film morphologies. (a) Energy-loss spectrum for neat IDIC(green), BDT-RO(red) and BDT-RN(blue), respectively. (b) BDT-RO EELS mapping in optimized blends of BDT-RO:IDIC; (c) IDIC EELS mapping in optimized blends of BDT-RO:IDIC; (d) BDT-RN EELS mapping in optimized blends of BDT-RN:IDIC; (e) IDIC EELS mapping in optimized blends of BDT-RN:IDIC.

12. Grazing Incidence Wide-angle X-ray Scattering

Silicon substrates were sonicated (Branson 5510) for 15 min each in successive baths of acetone and isopropanol. The substrates were then dried with pressurized nitrogen before being exposed to the UV−ozone plasma for 15 min. The BHJ layers were prepared following methods described in Section 6. Device Fabrication.

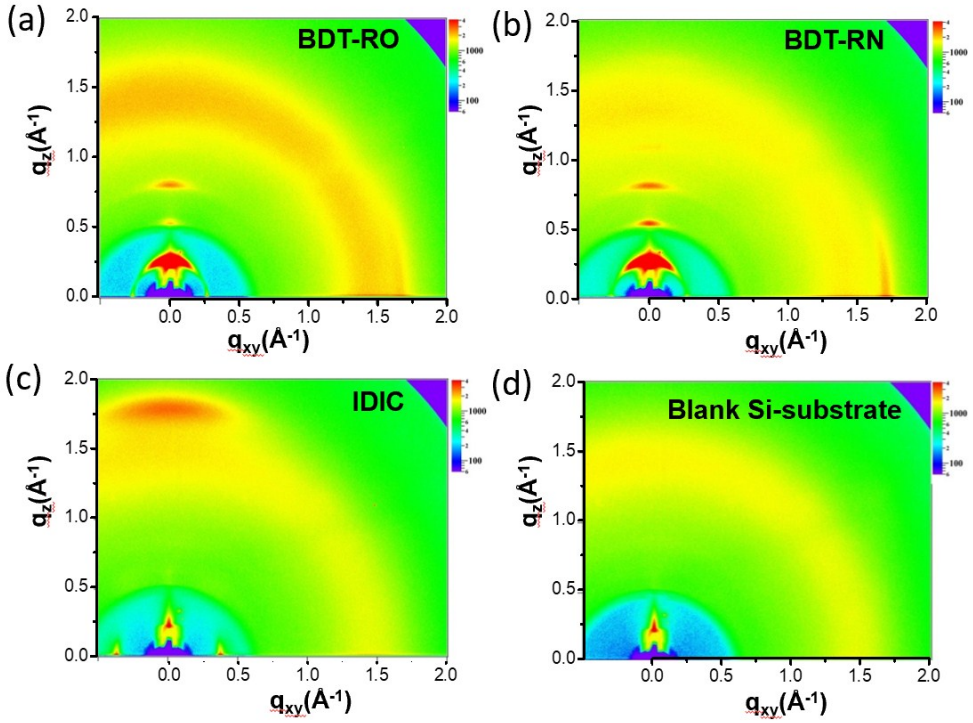

Figure S9. 2D GIWAXS patterns for the films (a) BDT-RO, (b) BDT-RN (c) IDIC (d) Blank Si-substrate.

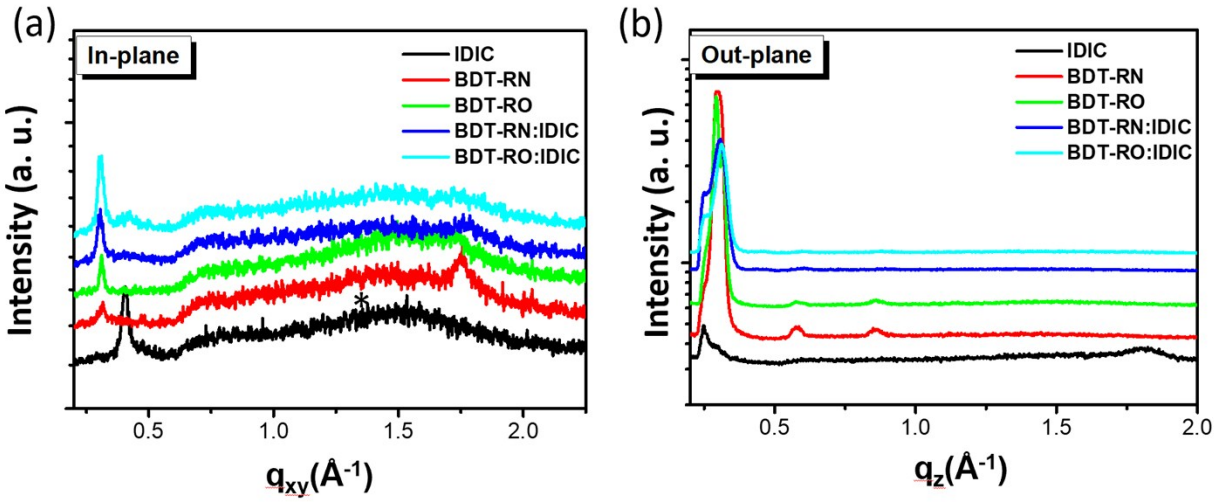

Figure S10. GIWAX scattering profiles (a) in-plane and (b) out-of-plane for films BDT-RO, BDT-RN, IDIC, BDT-RN:IDIC and BDT-RO:IDIC. All the films were spin coated on the Si-substrate.

Table S2. The data extracted from the in-plane and out-of-plane from GIWAXS images for the pristine (IDIC, BDT-RN and BDT-RO) and blend (BDT-RN:IDIC and BDT-RO:IDIC) films

	In-plane diffraction				**Out-of-plane diffraction**		
System	peaks	q (Å^{-1})	d-spacing (Å)	**Sample**	Characteristics	q (Å^{-1})	d-spacing (Å)
IDIC	100	0.404	15.55	**IDIC**	010	1.84	3.415
BDT-RN	100	0.316	19.88	**BDT-RN**	100	0.302	20.8
	010	1.757	3.57		200	0.576	10.9
					300	0.856	7.34
BDT-RO	100	0.311	20.2	**BDT-RO**	100	0.318	19.75
	010	1.721	3.62		200	0.579	10.87
					300	0.861	7.29
BDT-RN:IDIC	BDT-RN (100)	0.3041	20.66	**BDT-RN:IDIC**	BDT-RN (100)	0.306	20.53
	BDT-RN (010)	1.757	3.58		BDT-RN (200)	0.601	10.4
	IDIC (100)	0.409	15.36		BDT-RN (300)	----	---
BDT-RO:IDIC	BDT-RO (100)	0.308	3.25	**BDT-RO:IDIC**	BDT-RO (100)	0.310	20.27
	BDT-RO (010)	----	-----		BDT-RO (200)	0.605	10.39
	IDIC (100)	0.417	15.07		BDT-RO (300)	0.888	7.07

Table S3. The calculated full width at half-maximum (FWHM) and coherence from the diffraction peaks in the in-plane direction of pristine (IDIC, BDT-RN and BDT-RO) and blend (BDT-RN:IDIC and BDT-RO:IDIC) films.

System	**In-plane q (Å^{-1})**	**FWHM (Å^{-1})**	**Coherence length (nm)**
BDT-RN	0.316	0.0315	17.9
	1.757	0.4511	12.53
BDT-RO	0.311	0.01912	29.7
	1.721	0.0802	7.04
BDT-RN:IDIC	0.3041	0.2591	21.8
BDT-RO:IDIC	0.308	0.02623	21.5

Table S4. The calculated full width at half-maximum (FWHM) and coherence from the diffraction peaks in the out-of-plane direction of pristine (IDIC, BDT-RN and BDT-RO) and blend (BDT-RN:IDIC and BDT-RO:IDIC) films.

System	Out-of-plane q ($Å^{-1}$)	FWHM ($Å^{-1}$)	Coherence length (nm)
BDT-RN	0.576	0.04176	13.5
BDT-RO	0.579	0.06447	8.76
BDT-RN:IDIC	0.601	0.07604	7.43
BDT-RO:IDIC	0.605	0.06056	9.332

13. SCLC Measurements

SCLC mobility was measured using a diode configuration of ITO/PEDOT:PSS/ active layer /MoO_3/Ag for hole and ITO/ZnO/DPO/active layer/DPO/Ag for electron by taking the dark current density in the range of -0.5-5 V and fitting the results to a space charge limited form, where SCLC is described by:

$$J = \frac{9\varepsilon_0\varepsilon_\gamma\mu_0 V^2}{8L^3} exp\left(0.89\beta\sqrt{\frac{V}{L}}\right)$$

where J is the current density, L is the film thickness of the active layer, μ_0 is the hole or electron mobility, ε_r is the relative dielectric constant of the transport medium, ε_0 is the permittivity of free space (8.85×10^{-12} F m^{-1}), V (= V_{appl} - V_{bi}) is the internal voltage in the device, where V_{appl} is the applied voltage to the device and V_{bi} is the built-in voltage due to the relative work function difference of the two electrodes.

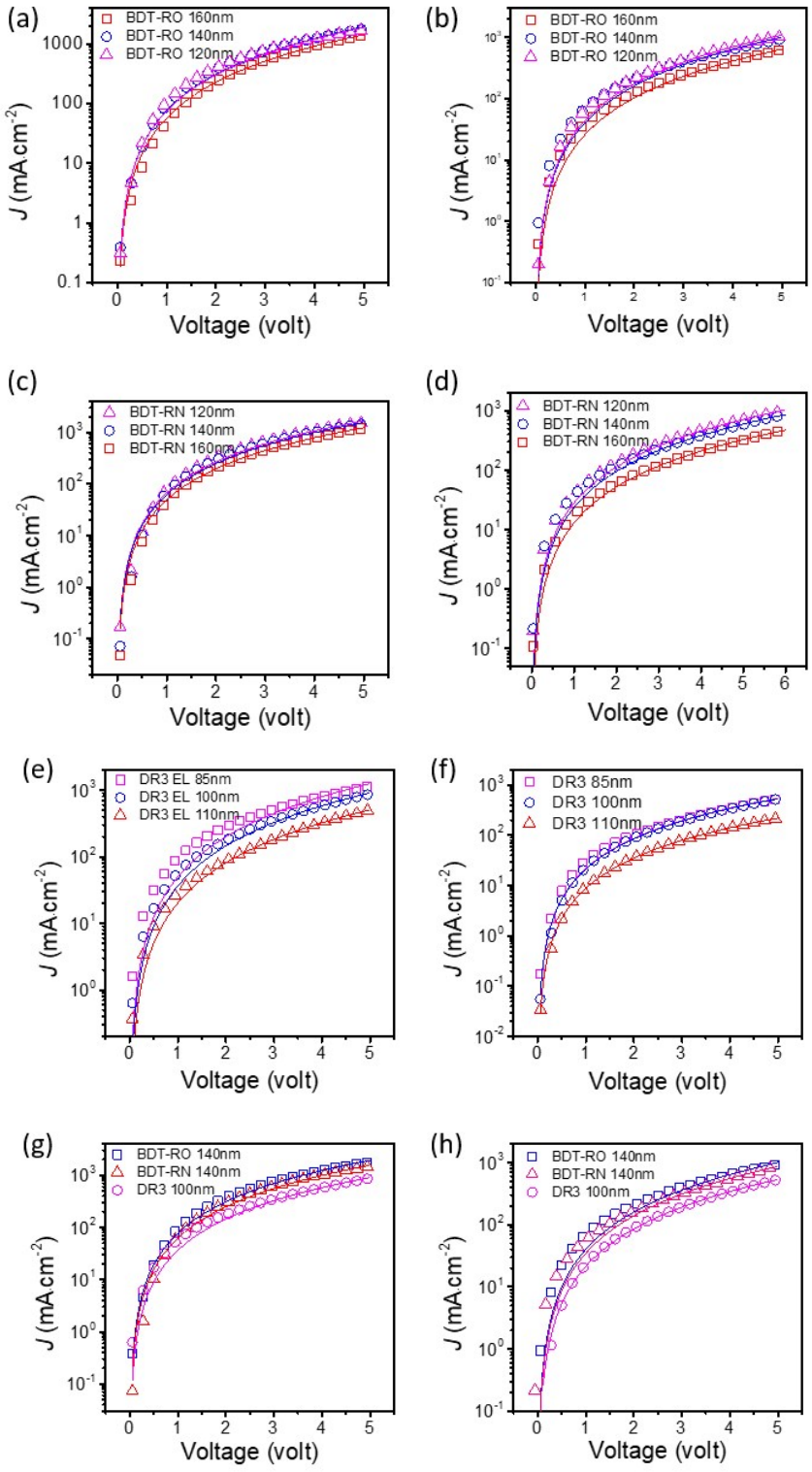

Figure S11. Experimental dark-current densities for optimized condition of BDT-RO:IDIC, BDT-RN:IDIC and DR3TBTT:IDIC devices with various thickness of electron-only (a, c, e) and hole-only (b, d, f) devices. BDT-RO:IDIC, BDT-RN:IDIC and

DR3TBTT:IDIC devices with optimized thickness of electron-only (g) and hole-only (h) devices.

Table S5. Summary of carrier mobilities.

Optimized Condition	μ_h[cm^2 V^{-1} s^{-1}]	μ_e[cm^2 V^{-1} s^{-1}]	μ_e/μ_h
BDT-RO:IDIC=1:0.8	3.24×10^{-4}	6.45×10^{-4}	1.99
BDT-RN:IDIC=1:0.8	1.87×10^{-4}	5.44×10^{-4}	2.91
DR3TBTT:IDIC=1:1	5.19×10^{-5}	1.05×10^{-4}	2.02

14. Solution NMR Spectra

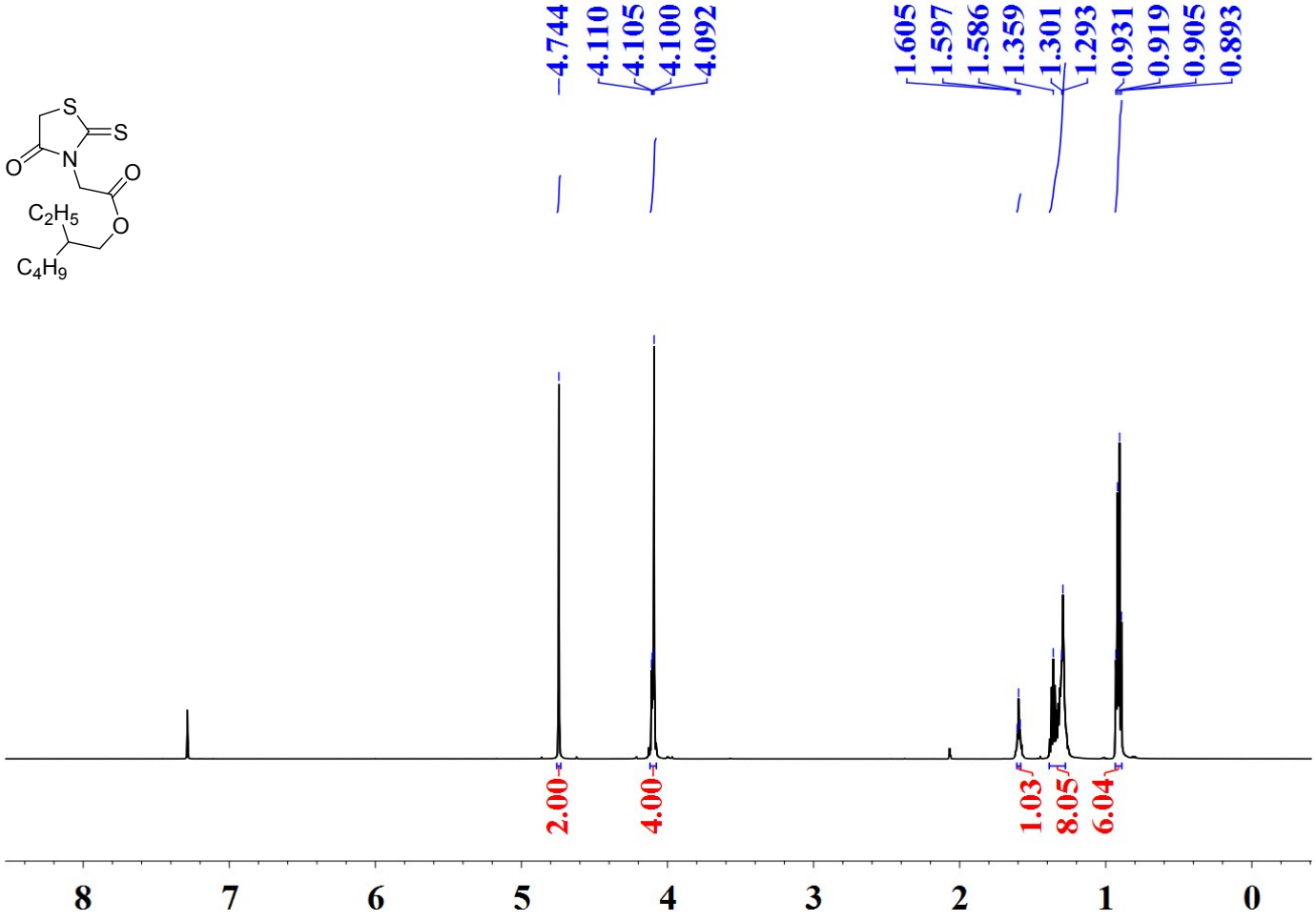

Figure S12. ^{1}H NMR spectrum of **1** in $CDCl_3$.

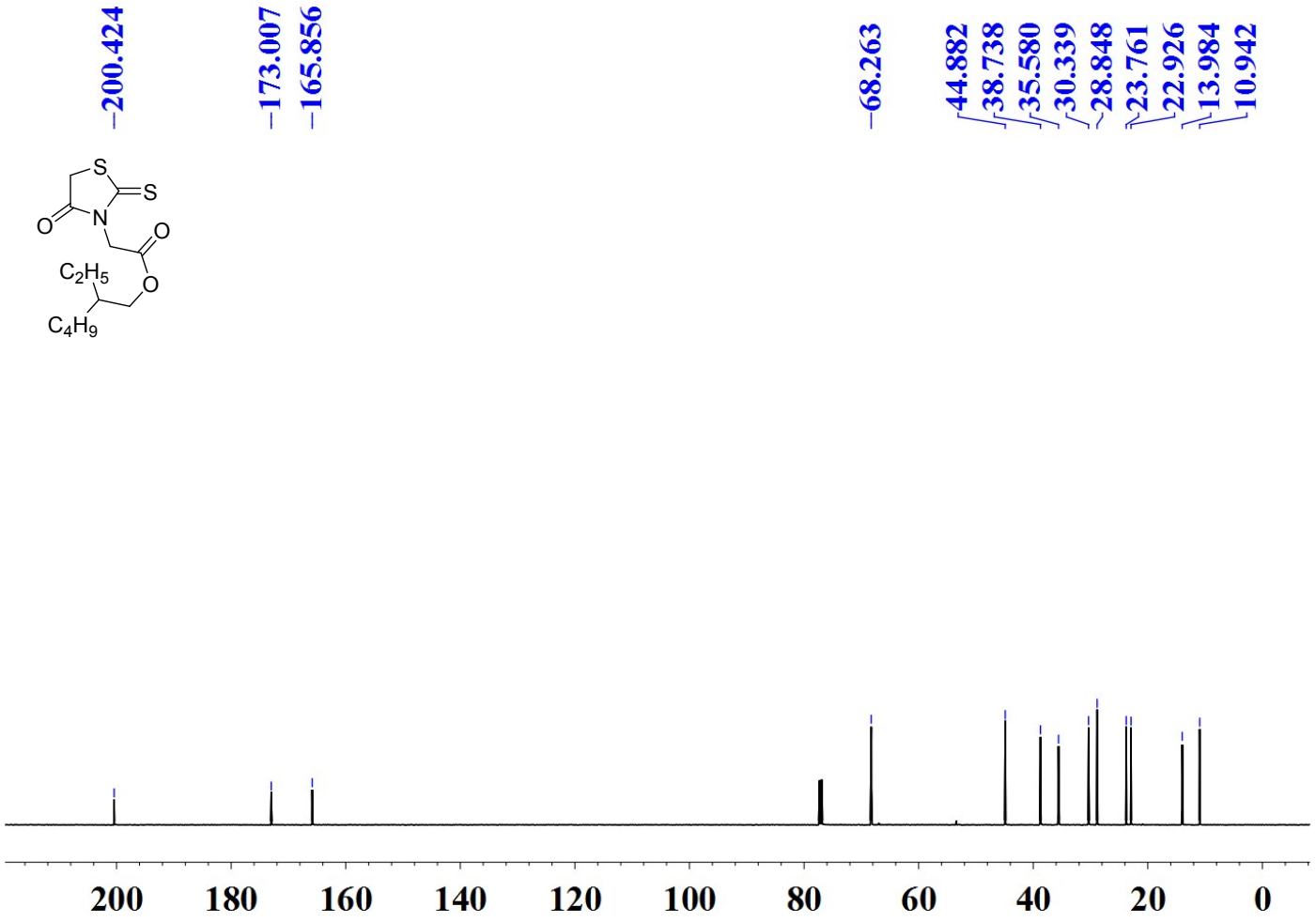

Figure S13. ^{13}C NMR spectrum of **1** in $CDCl_3$.

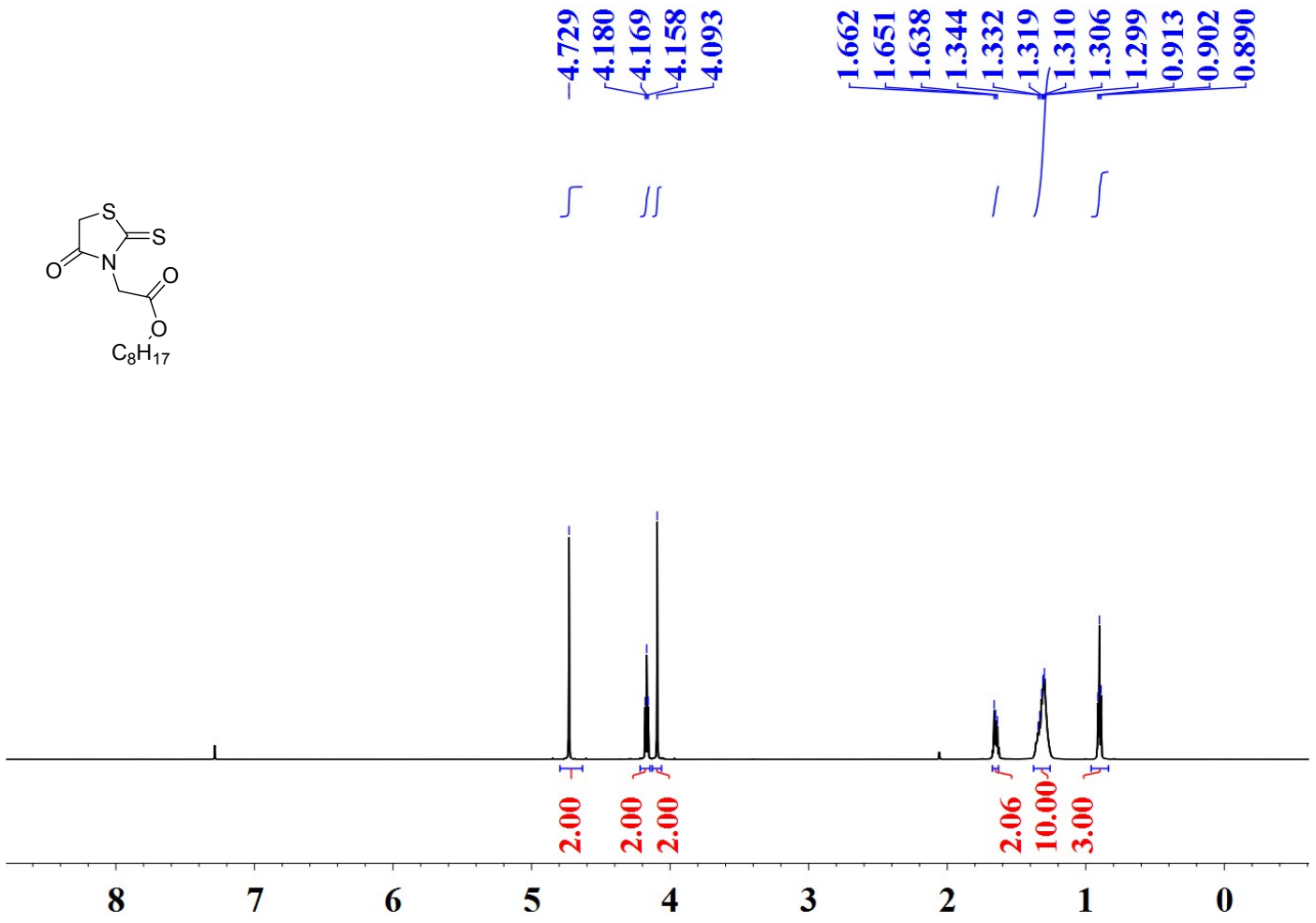

Figure S14. ^{1}H NMR spectrum of **2** in $CDCl_3$.

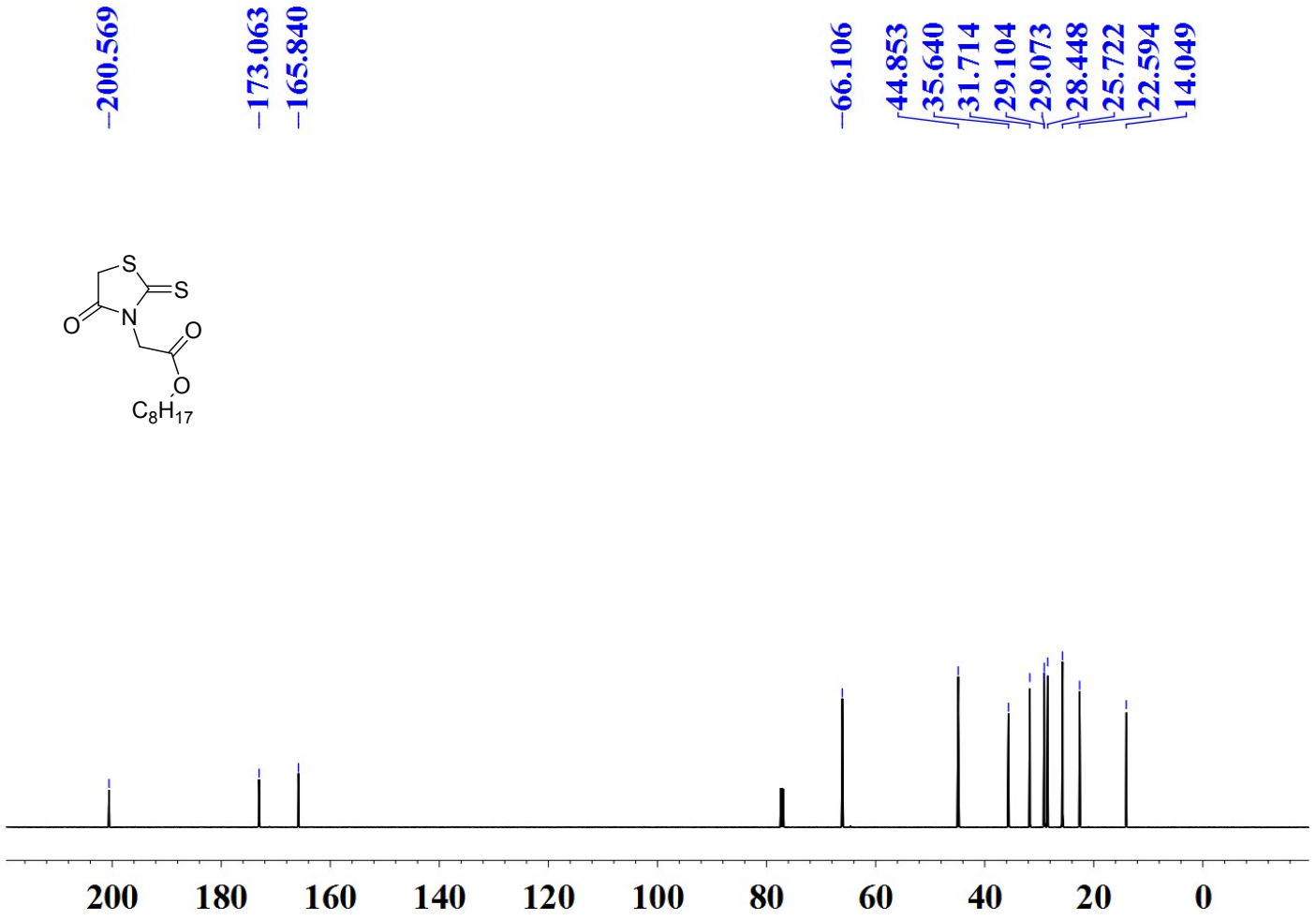

Figure S15. ^{13}C NMR spectrum of **2** in $CDCl_3$.

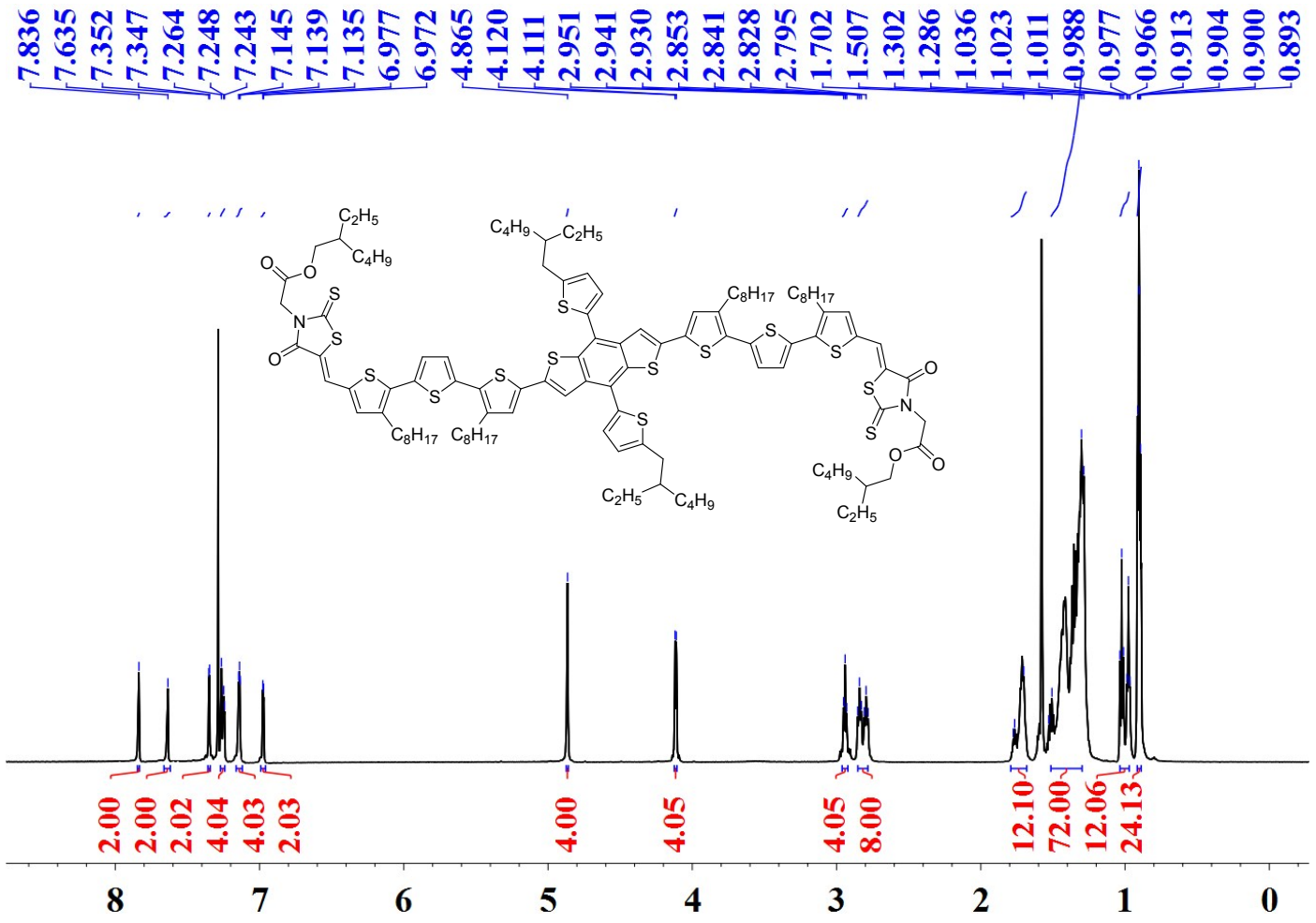

Figure S16. ^{1}H NMR spectrum of **BDT-RO** in $CDCl_3$.

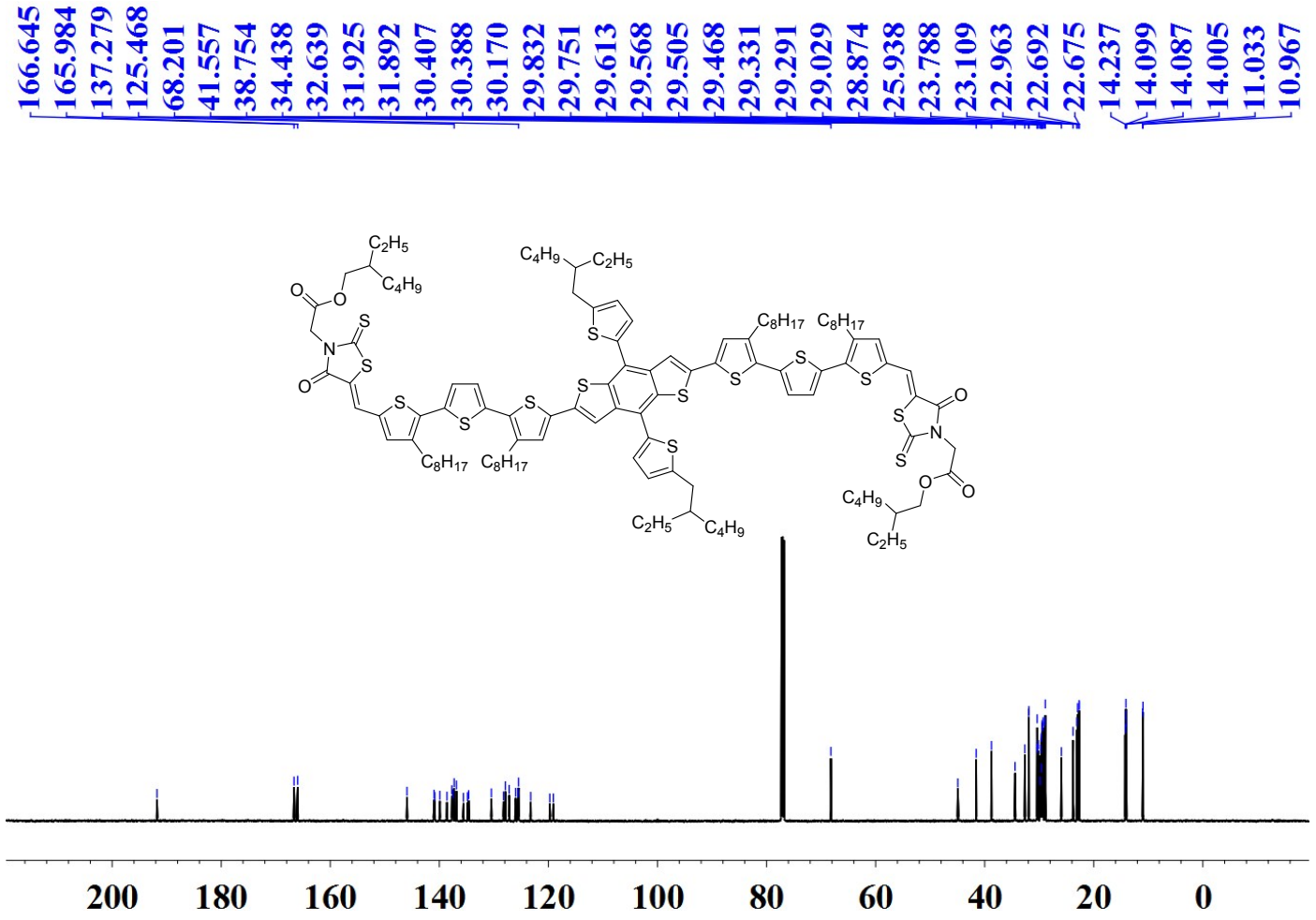

Figure S17. ^{13}C NMR spectrum of **BDT-RO** in $CDCl_3$.

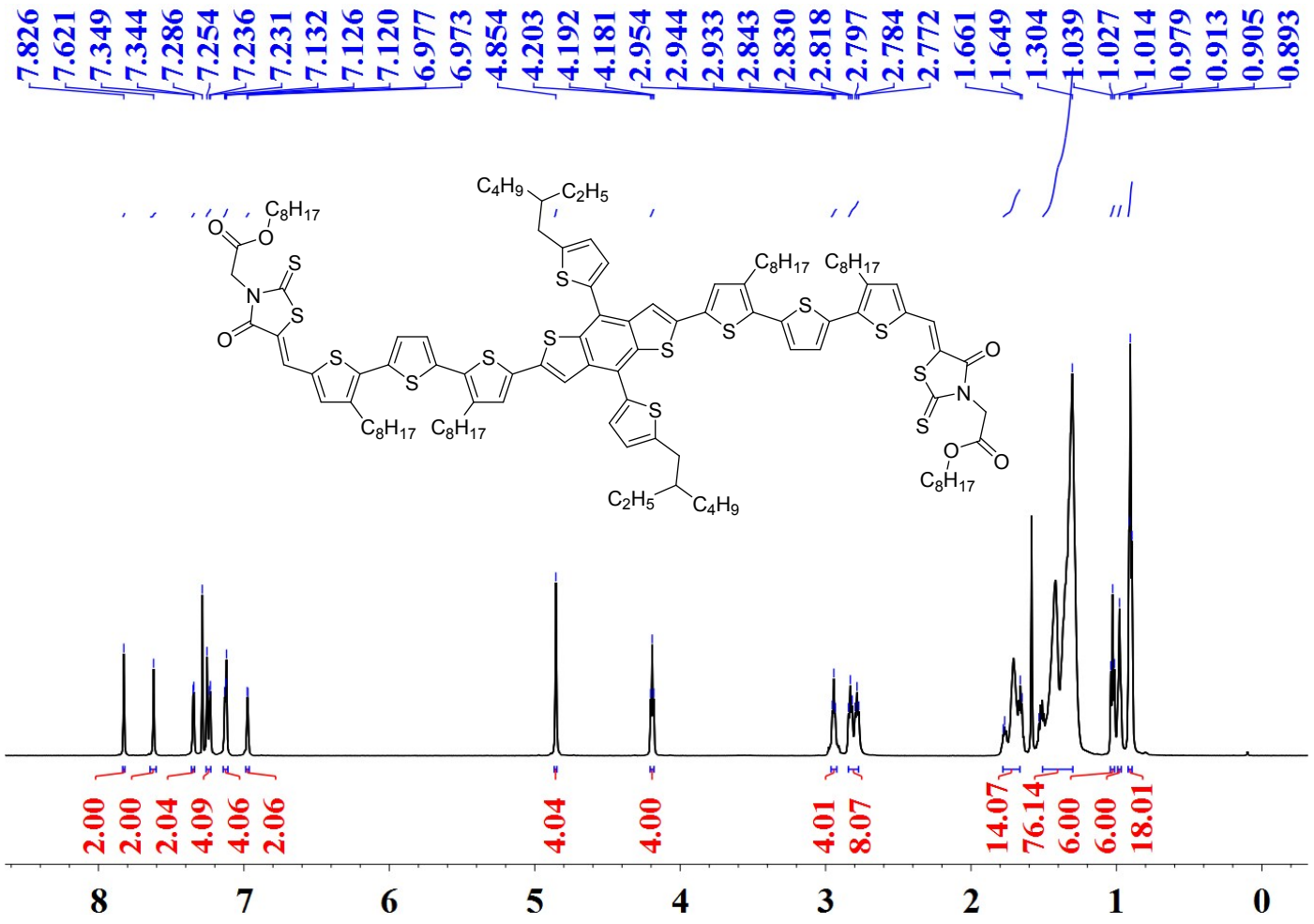

Figure S18. ^{1}H NMR spectrum of **BDT-RN** in $CDCl_3$.

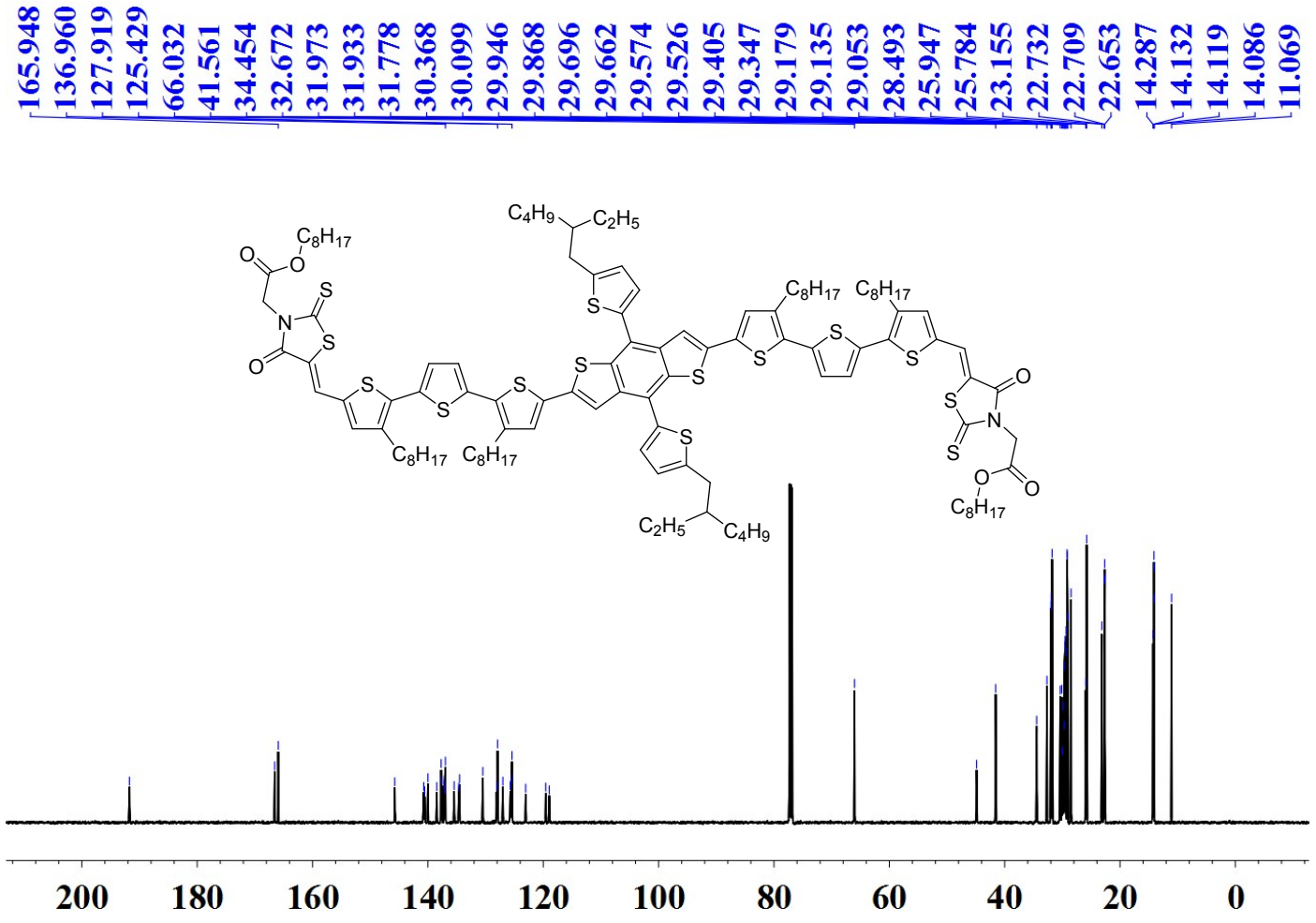

Figure S19. ^{13}C NMR spectrum of **BDT-RN** in $CDCl_3$